frontiers | Frontiers in Physics

TYPE Original Research
PUBLISHED 05 January 2026
DOI 10.3389/fphy.2025.1673486



OPEN ACCESS

EDITED BY
Stefan C. Müller,
Otto von Guericke University
Magdeburg, Germany

REVIEWED BY
Hisashi Hayashi,
Japan Women's University, Japan
Njitacke Tabekoueng Zeric,
University of Buea, Cameroon

*CORRESPONDENCE
Layla Badr,
lbadr@ndu.edu.lb

RECEIVED 25 July 2025
REVISED 23 October 2025
ACCEPTED 02 December 2025
PUBLISHED 05 January 2026

CITATION
Badr L (2026) Spatiotemporal dynamics in silver thiosulfate, silver sulfide reaction-diffusion system.
*Front. Phys.* 13:1673486.
doi: 10.3389/fphy.2025.1673486



# Spatiotemporal dynamics in silver thiosulfate, silver sulfide reaction-diffusion system

Layla Badr*

Department of Sciences, Faculty of Natural and Applied Sciences, Notre Dame University – Louaize, Zouk Mosbeh, Lebanon

Liesegang pattern formation is a self-organizing phenomenon governed by diffusion and reaction kinetics generally in a porous matrix. This study investigates the transient precipitation dynamics of silver thiosulfate and its subsequent formation into silver sulfide Liesegang pattern within gelatin matrices through the diffusion of sodium thiosulfate into silver nitrate. The interplay between the decomposition of $Ag_2S_2O_3$ to $Ag_2S$ and its dissolution into soluble $[Ag(S_2O_3)_2]^{3-}$ complex ion under excess thiosulfate produces $Ag_2S$ periodic patterned bands. The migration extent of the $Ag_2S_2O_3$ band increases with increasing concentration gradient and its width increases with increasing gelatin percentage. The $Ag_2S$ bands morphology and clarity are primarily regulated by the gelatin structure and solvent polarity, with potassium fluoride, an inert salt contributing to sharper boundaries through increased complex ion and colloid stability. The system successfully isolates the thermodynamically unstable silver thiosulfate, produces in some cases equidistant silver sulfide Liesegang pattern for the 2.5% gelatin systems, and reveals that pattern morphology and spacing can be tuned by modifying experimental conditions. In addition, this study is significant for understanding a unique class of Liesegang patterns wherein the kinetics of dissolution and dissociation are alternating in response to the diffusion of a counter ion that initially forms a precipitate at the reaction front.

KEYWORDS

**self-organization, reaction-diffusion kinetics, Liesegang patterns, silver thiosulfate, silver sulfide**

## 1 Introduction

Self-organized systems are systems that spontaneously develop ordered structures through internal interactions. Self-organization emerges without external control in systems that are maintained far from equilibrium in a variety of reactor configurations [1, 2]. The self-organization phenomenon attracts scientists for its applications in a variety of fields like geology and earth sciences, biology and biochemistry, and materials science and nanotechnology [3–5].

Liesegang banding is an example of self-organized spontaneous phenomenon where periodic, patterned precipitate bands form in porous media due to the reciprocal and dynamic interaction between diffusion and chemical reactions. The reagents are initially separated with one of them, the inner electrolyte, dissolved and spread homogeneously in a porous stagnant medium and the other, the outer electrolyte, in an aqueous medium that is made to diffuse into the immobile medium. These reaction-diffusion mediated bands often appear as parallel lines or concentric rings, and were

first observed by the German chemist Raphael Eduard Liesegang [6]. The periodicity of the typical Liesegang patterns shows a geometric progression known as the Spacing law. The Spacing law is an empirical law given by

$$\lim_{n\to\infty} \frac{x_{n+1}}{x_n} = 1 + p$$

where $x_n$ and $x_{n+1}$ are the distance of the $n^{\text{th}}$ and $(n+1)^{th}$ bands measured from the interface between the media containing the reacting electrolytes. And $p$ is the spacing coefficient, which is constant at large values of $n$. The inter band spacing given by

$$\Delta x_n = x_{n+1} - x_n$$

generally increases with increasing $n$ in regular Liesegang patterns. However, when $\Delta x_n$ is constant or decreasing with increasing $n$; equidistant [7, 8] and revert spacing [9, 10] (invert) Liesegang patterns are obtained. Other empirical rules that have been used in the analysis of Liesegang patterns are the Width law

$$w_n \propto x_n^{\alpha}$$

and the Time law;

$$x_n \propto t_n^{1/2}$$

$w_n$, the width of the $n^{\text{th}}$ band usually increases linearly with increasing $x_n$ for the regular type Liesegang patterns. When α is close to unity, the distribution of the precipitate in consecutive bands is uniform, and the mass conservation is satisfied [11]. The relationship between $x_n$ and the time at which the $n$ band appears $t_n$, in the Time law is a consequence of the diffusive nature of the mechanism where the distance traversed through diffusion is linearly proportional to the square root of the time [12].

The periodicity of Liesegang patterns can be controlled by physical and chemical conditions like the porosity of the reaction medium [13, 14], direct and alternating electric fields [15], pH [16], and solvent polarity [17]. Understanding the mechanisms behind Liesegang banding provides insight into pattern formation in nature [18, 19] and helps model processes such as the fabrication of surfaces with periodic structures [20, 21] with precise spacing for the advancement in sensors, semiconductors, catalysis, and photonic materials.

The two most widely accepted models for Liesegang pattern formation are the prenucleation and postnucleation models or a combination thereof [22, 23]. The main difference between the two models lies in the specific steps of the formation of the periodic patterns. In the prenucleation model, as the outer electrolyte diffuses into the inner electrolyte, nucleation and particle growth occur in the region at which the ion concentration product exceeds the solubility product constant, $K_{sp}$ of the corresponding salt. As a result of nucleation and particle growth, the ions present in front of the reaction front diffuse backward due to concentration gradient. This back-diffusion forms a depleted region in which the concentrations of ions cannot exceed the solubility product constant. As a result, the formation of repeated particle and depleted zones produces Liesegang patterns. In contrast, according to the postnucleation model, the patterns are formed following the onset of homogeneous nucleation and particle growth. In the postnucleation model, the proceeding reaction front leaves a constant concentration of particles. Then the spontaneous arousal of repeated particle aggregations and depleted zones is followed due to thermodynamic stability or competitive growth and dissolution of particles of different sizes within the particle distribution.

In the studied system, the thiosulfate ions $S_2O_3^{2-}$ from $Na_2S_2O_3{\cdot}5H_2O$ aqueous solution is made to diffuse into a porous gelatin medium containing silver ions $Ag^+$ from silver nitrate $AgNO_3$. The following reaction first takes place;

$$2\,AgNO_3(aq) + Na_2S_2O_3(aq) \rightarrow Ag_2S_2O_3(s) + 2\,NaNO_3(aq)$$

forming the insoluble silver thiosulfate $Ag_2S_2O_3$ white precipitate. Silver thiosulfate is unstable in aqueous solution and decomposes to form silver sulfide $Ag_2S$ and sulfuric acid.

$$Ag_2S_2O_3(s) + H_2O(l) \rightarrow Ag_2S(s) + H_2SO_4(aq)$$

However, in excess $Na_2S_2O_3$, the precipitate $Ag_2S_2O_3$ dissolves forming the colorless soluble complex salt $Na_3$ $[Ag(S_2O_3)_2]$ sodium bis(thiosulfato) argentite, commonly known as sodium silver thiosulfate STS [24, 25].

$$Ag_2S_2O_3(s) + \text{excess}\,Na_2S_2O_3(aq) \rightarrow Na_3[Ag(S_2O_3)_2](aq)$$

When mixing takes place in an aqueous solution, $Ag_2S_2O_3$ cannot be readily isolated since it either readily decomposes to $Ag_2S$, or if excess sodium thiosulfate is present, the soluble complex $Na_3[Ag(S_2O_3)_2]$ is formed. The reaction with excess $Na_2S_2O_3$ prevents the precipitation of the silver ion, making $Ag^+$ soluble again as the complex ion $[Ag(S_2O_3)_2]^{3-}$. In solution, bis(thiosulfato) argentite ion has many uses. For example, in plant biology it inhibits ethylene, a hormone that influences flowering and senescence. By blocking ethylene's effect, $[Ag(S_2O_3)_2]^{3-}$ can extend flower longevity and promote male flower development [26]. Another use is in cancer studies, where $[Ag(S_2O_3)_2]^{3-}$ solution exhibited an anticancer activity through ROS-induced mechanisms, and its cytotoxicity is highly selective to MCF-7 breast cancer cells [27]. While bis(thiosulfato) argentite complex ion is active when in aqueous solution, silver sulfide is more relevant in natural rocks in the form of acanthite and argentite. Silver sulfide forms hydrothermal veins within host rocks and is the main viable silver source after native silver [28, 29]. $Ag_2S$ is a flexible thermoelectric material with a high Seebeck coefficient, tunable electrical property, low thermal conductivity, and high ductility suitable for a wide range of applications [30–32]. When periodically precipitated within hydrogels, $Ag_2S$ can potentially impart localized and controlled inhibition of bacterial or fungal growth and thus lead to site-specific antimicrobial action with a regulated release of silver ions to reduce toxicity concerns.

The precipitation–dissolution–decomposition kinetics coupled to transport in the silver thiosulfate/silver sulfide system led to a number of interesting patterns in this study. The effects of changing (1) the porosity of the reaction medium by changing the gelatin percentage, (2) the outer electrolyte $Na_2S_2O_3{\cdot}5H_2O$ concentration, and (3) the presence of an inert salt potassium fluoride KF, on the

morphology of the patterns were studied. Experimental conditions were changed accordingly to understand the dynamics of the pattern formation mechanism.

Finally, the mechanism studied which is based on thermodynamic instability and kinetic control is not classical in Liesegang pattern formation and can help understand natural like structures in rocks and minerals. The silver sulfide Liesegang bands involve the decomposition of silver thiosulfate which mimics transient intermediates in mineral-forming environments where sulfur and silver coexist. In addition, the study was successful in isolating the thermodynamically unstable $Ag_2S_2O_3$ precipitate and the results will have implications on the design strategies of silver thiosulfate, silver sulfide materials.

## 2 Materials and methods

Gel solutions of 0.01 M silver nitrate were prepared by dissolving the desired amounts of reagent grade $AgNO_3$ (Alfa Aesar, 99.9+%, crystalline) and gelatin powder (Sigma Aldrich) in distilled water. The following percentages of gelatin were prepared: 2.5%, 5%, 7.5%, 10%, and 12.5%. Also, gel solutions with 0.01 M and 0.1 M potassium fluoride KF and 0.01 M $AgNO_3$ in 2.5%, 7.5%, and 12.5% gel media were prepared. The gel solutions were heated and stirred until they became homogeneous then filled up to 15 cm of 20 cm glass tubes with 0.3 cm inner diameter. The solutions in the glass tubes were then left to gelify overnight at room temperature and in the dark to avoid the photo-reduction of silver ions [33]. On the second day, the upper level of the gelled silver nitrate (inner electrolyte) solutions in the tubes were marked and sodium thiosulfate $Na_2S_2O_3$ (outer electrolyte) solutions were added to fill the empty upper 5 cm in the glass tubes. The mark indicates the diffusion interface. The following concentrations of sodium thiosulfate from $Na_2S_2O_3{\cdot}5H_2O$ (VWR Chemicals, 99.5%) were used; 0.1 M, 1 M, and 2.5 M. The instant at which sodium thiosulfate touched the inner electrolyte gel solution marked the beginning of the experiment. The outer electrolyte solutions were allowed to diffuse down into the inner $AgNO_3$ and $AgNO_3$ plus KF electrolyte gel solutions in a vertical direction. The experimental tubes were left in the dark at 20 °C. Images of the systems were taken every 24 hours for 8 days and image analysis was done using ImageJ [34].

## 3 Results

Figure 1 shows the patterns with 0.01 M $AgNO_3$ and 0.1 M $Na_2S_2O_3{\cdot}5H_2O$ at all gelatin percentages; with and without KF on Day 3 as examples. A white $Ag_2S_2O_3$ band is seen at the reaction front tailed by $Ag_2S$ precipitate and $Na_3[Ag(S_2O_3)_2]$ complex solution. The silver thiosulfate precipitate band existed for the 8 days' period of the experiments, and clear boundaries between the $Ag_2S$ band and $Na_3$ $[Ag(S_2O_3)_2]$ solution are obtained best for the 2.5% gelatin systems. To study the migration and growth kinetics of the $Ag_2S_2O_3$ precipitate band, the migration extent and the width of the band are investigated. The variation of the migration extent $d$ with time and with $Na_2S_2O_3{\cdot}5H_2O$ concentration are given in Figures 2A,B. In Figure 2A an outer electrolyte concentration of 1 M is selected and the variation of $d$ with time is shown for systems with 2.5%, 7.5%, and 12.5% gelatin percentages with no KF. In Figure 2B the variation of $d$ with $Na_2S_2O_3{\cdot}5H_2O$ concentration on days 2, 4, 6, and 8 is shown. The systems selected for instance for the data points in Figure 2B have a 7.5% gelatin percentage and no potassium fluoride added. As for the $Ag_2S_2O_3$ band width, Figures 3A–C shows the variation of the width with time for all the systems studied.

The colour intensities of the reaction tubes are analysed after the appropriate scaling of the images in ImageJ. Intensity profile unveil the distribution of pixel intensity values along the line of the experimental tube from the inner/outer electrolyte interface to the reaction front. The profile consists of a plot where the x-axis represents the distance along the experimental tube from the interface and the y-axis represents the corresponding intensity values. Figure 4 provides the intensity profile for the 7.5% gelatin, 1 M $Na_2S_2O_3{\cdot}5H_2O$, and 0.1 M kF on Days 4, 5,

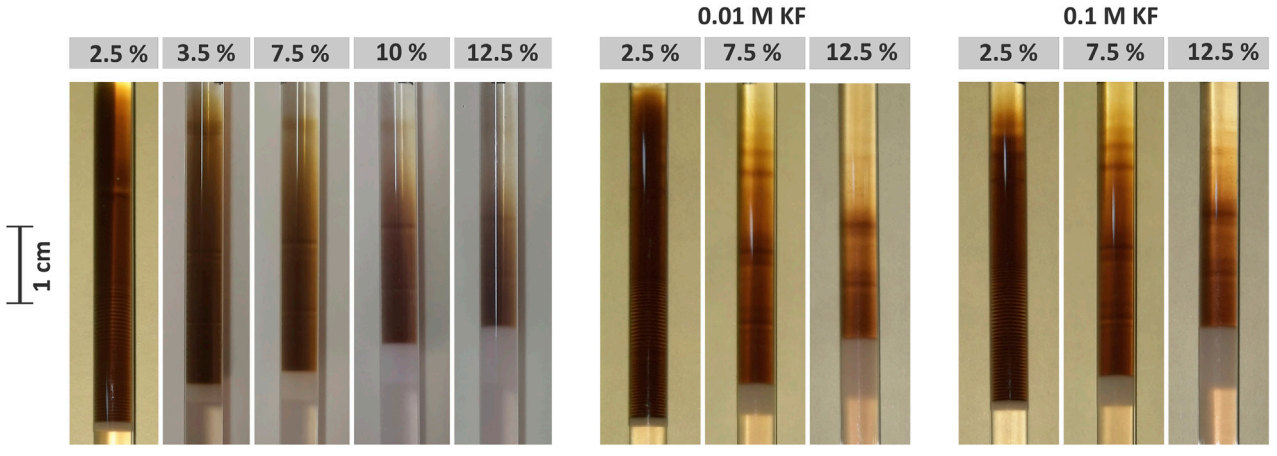


FIGURE 1
$Ag_2S_2O_3/Ag_2S$ patterns with 0.01 M $AgNO_3$ and 0.1 M $Na_2S_2O_3{\cdot}5H_2O$ at the indicated gelatin percentages on Day 3 with and without KF.

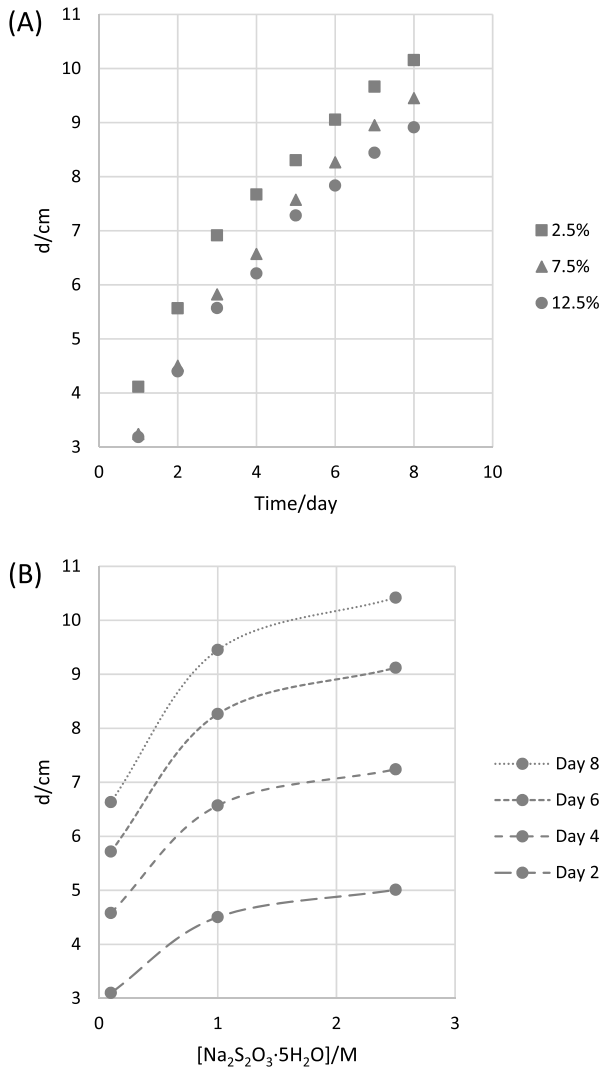


FIGURE 2
**(A)** The variation of the migration extent *d* with time for the 2.5%, 7.5%, and 12.5% gelatin percentages with no KF and 1 M $Na_2S_2O_3{\cdot}5H_2O$ outer electrolyte concentration and **(B)** The variation of the migration extent *d* with the concentration of $Na_2S_2O_3{\cdot}5H_2O$ on days 2, 4, 6, and 8 for the 7.5% gelatin with no KF system (the lines are drawn as an aid to the eye, no curve fitting applies). The sizes of the errors on the measurements are smaller than the sizes of the data points.

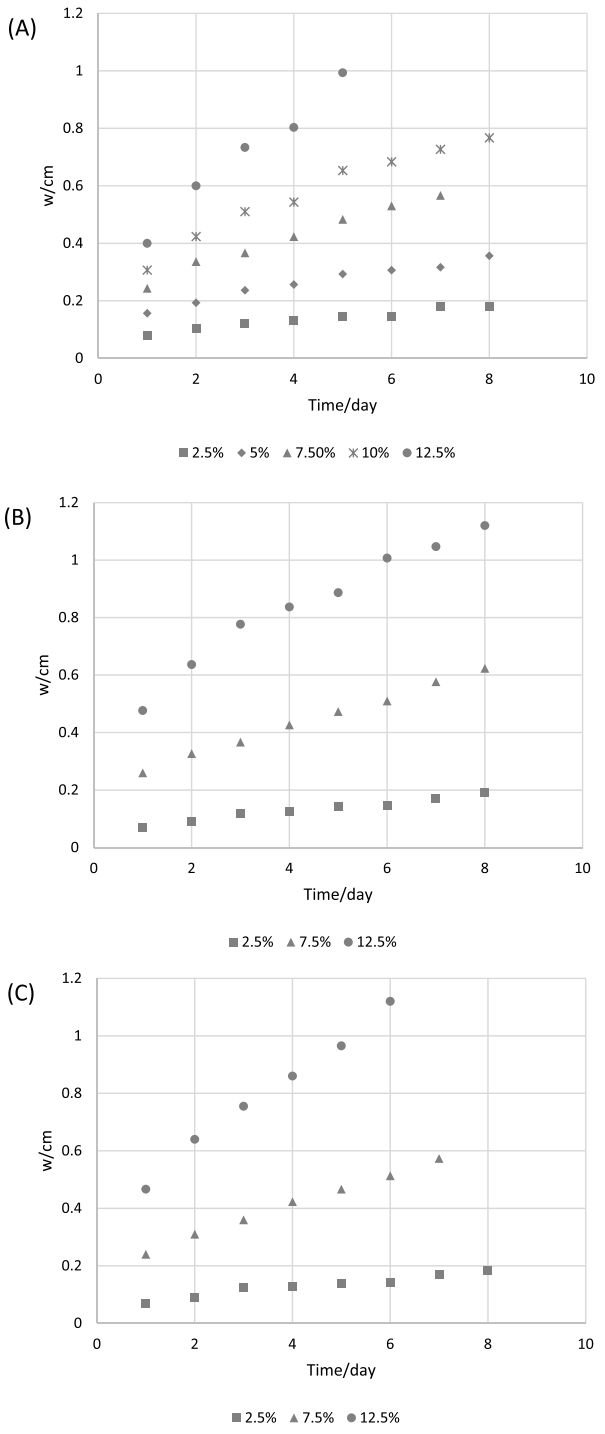


FIGURE 3
The variation of the width of $Ag_2S_2O_3$ precipitate band with time. **(A)** for 2.5%, 5%, 7.5%, 10%, and 12.5% without KF **(B)** for 2.5%, 7.5%, and 12.5% with 0.01 M kF and **(C)** for 2.5%, 7.5%, and 12.5% with 0.1 M kF. The sizes of the errors on the measurements are smaller than the sizes of the data points. The value for the width for a specific percentage at a specific time is an average width for the three systems with different $Na_2S_2O_3{\cdot}5H_2O$ concentrations.

and 6. While Figure 5 utilizes intensity profiles to precisely calculate the band width and inter band distance for 2.5% gelatin and 1 M $Na_2S_2O_3{\cdot}5H_2O$ systems on Day 3.

# 4 Discussion

## 4.1 Silver thiosulfate $Ag_2S_2O_3$

At the beginning of the experiment, the outer electrolyte sodium thiosulfate $Na_2S_2O_3$ solution starts diffusing in the gelatin because its concentration is greater than the concentration of the inner electrolyte silver nitrate $AgNO_3$ that is distributed homogeneously in the gelatin. At the solution/gel interface, the precipitation of silver thiosulfate $Ag_2S_2O_3$ occurs immediately and the precipitate band starts growing downward. Under the studied experimental conditions, the white $Ag_2S_2O_3$ is clearly distinguished as seen in Figure 1. Its formation is faster than its dissociation into

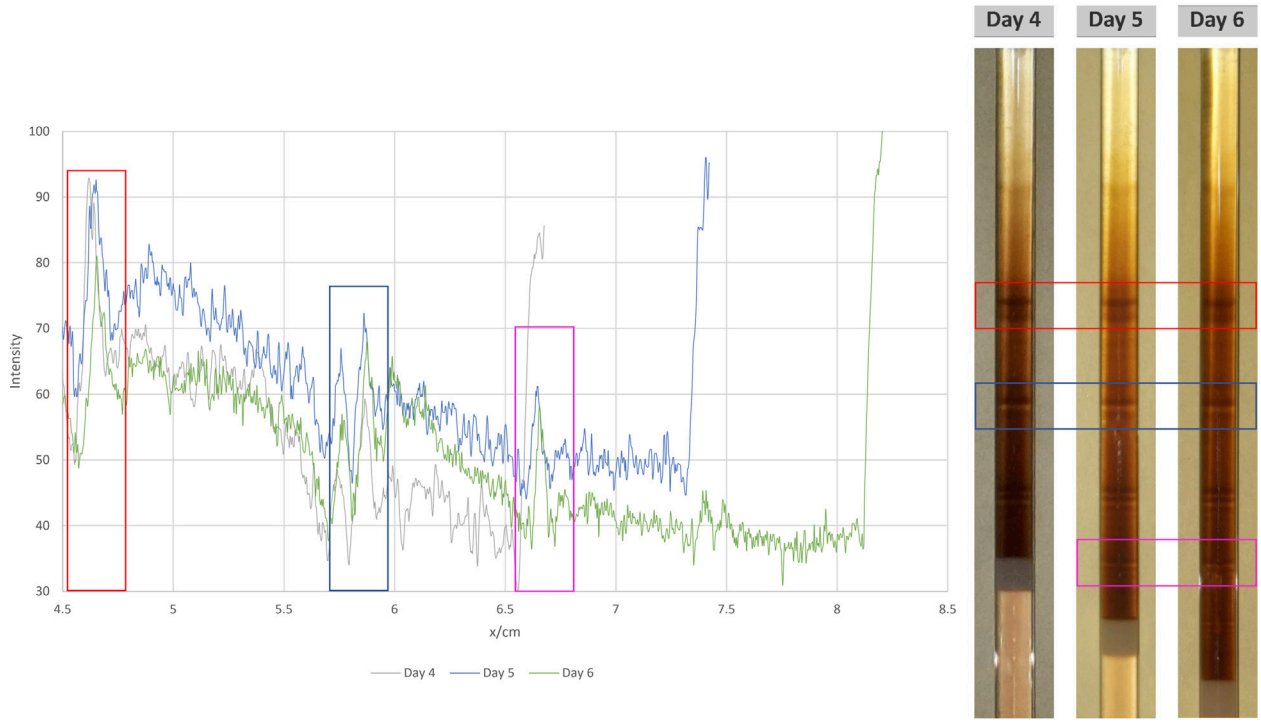


FIGURE 4
Intensity profile of the $Ag_2S_2O_3/Ag_2S$ pattern on Days 4, 5, and 6 for 7.5% gelatin, 1 M $Na_2S_2O_3{\cdot}5H_2O$, and 0.1 M kF system. The highlighted boxes show the static locations of the $Ag_2S$ precipitate bands.

silver sulfide $Ag_2S$ and its dissolution to bis(thiosulfato) argentite $[Ag(S_2O_3)_2]^{3-}$ complex ion by the diffusing sodium thiosulfate. As diffusion of the thiosulfate ions continues, silver thiosulfate is formed at the band front and either dissociated or dissolved in excess solvent at the band rear. The repetition of these processes lead to the migration of the white $Ag_2S_2O_3$ band down the reaction tube with time.

The progression of the reaction front is investigated by determining the variation of the distance $d$ between the inner/outer electrolyte interface and the band front as a function of time. Figure 2A shows $d$, the migration extent for the 2.5%, 7.5%, and 12.5% gelatin percentages with no KF and 1 M $Na_2S_2O_3{\cdot}5H_2O$ outer electrolyte concentration as an example. Results showed that $d$ continuously increases with time and is proportional to $t^{\alpha}$, with the exponent $\alpha$ close to 0.5 under all experimental conditions, thus satisfying the Time law. The values of the exponent $\alpha$ for all the systems are shown in Table 1. This square root time dependence of the propagation of the reaction-front suggests that the rate of formation of $Ag_2S_2O_3$ is controlled by diffusion [35]. In addition, the migration extent $d$ decreases with increasing gelatin percentage at the studied times, Figure 2A. This is expected because at higher percentages the gelatin matrix becomes tighter and the pore size becomes smaller thus reducing the mobility of the diffusing solution. However, a more pronounced decrease in $d$ at a given time appears as the concentration of the outer electrolyte $Na_2S_2O_3{\cdot}5H_2O$ decreases. Figure 2B shows the variation of the migration extent $d$ on days 2, 4, 6, and 8 for the systems with inner gelatin percentage of 7.5% and no KF as examples. This behavior relies on the concentration gradient between the inner electrolyte and the outer electrolyte. A large gradient creates a strong driving force that propels the sodium thiosulfate solution to move deeper into the gelatin medium. This driving force helps overcome resistance in the medium, thus allowing a more efficient diffusion when the gradient is high.

The width $w$ of the silver thiosulfate white band is found to increase with time and with gelatin percentage for systems with and without potassium fluoride as shown in Figures 3A–C. The increase of the band width with time suggests that the rate of $Ag_2S_2O_3$ formation at the band front is larger than the rate of its dissociation into $Ag_2S$ and dissolution into $[Ag(S_2O_3)_2]^{3-}$ at the band rear. Furthermore, by increasing the gelatin percentage, the gel surface area increases and the network becomes denser [36] thus creating more nucleation sites. Nucleation occurs when the $Ag_2S_2O_3$ salt molecule concentration reaches the nucleation threshold. A denser network leads to faster nucleation rate and thus larger number of small crystals dispersed in the polymer matrix [37, 38]; this behavior is reflected by the increase of the band width with gelatin percentage as seen in Figure 3. Results also show that irrespective of the concentration of the outer electrolyte the band width is the same for a given gelatin percentage with standard deviation for the width at the three different $Na_2S_2O_3{\cdot}5H_2O$ concentrations within the experimental measurement error. In addition, at most times, there is no pronounced effect of the presence and concentration of KF on the $Ag_2S_2O_3$ band width variation.

In summary, the concentration gradient between the inner electrolyte and the outer electrolyte primarily sets the pace of

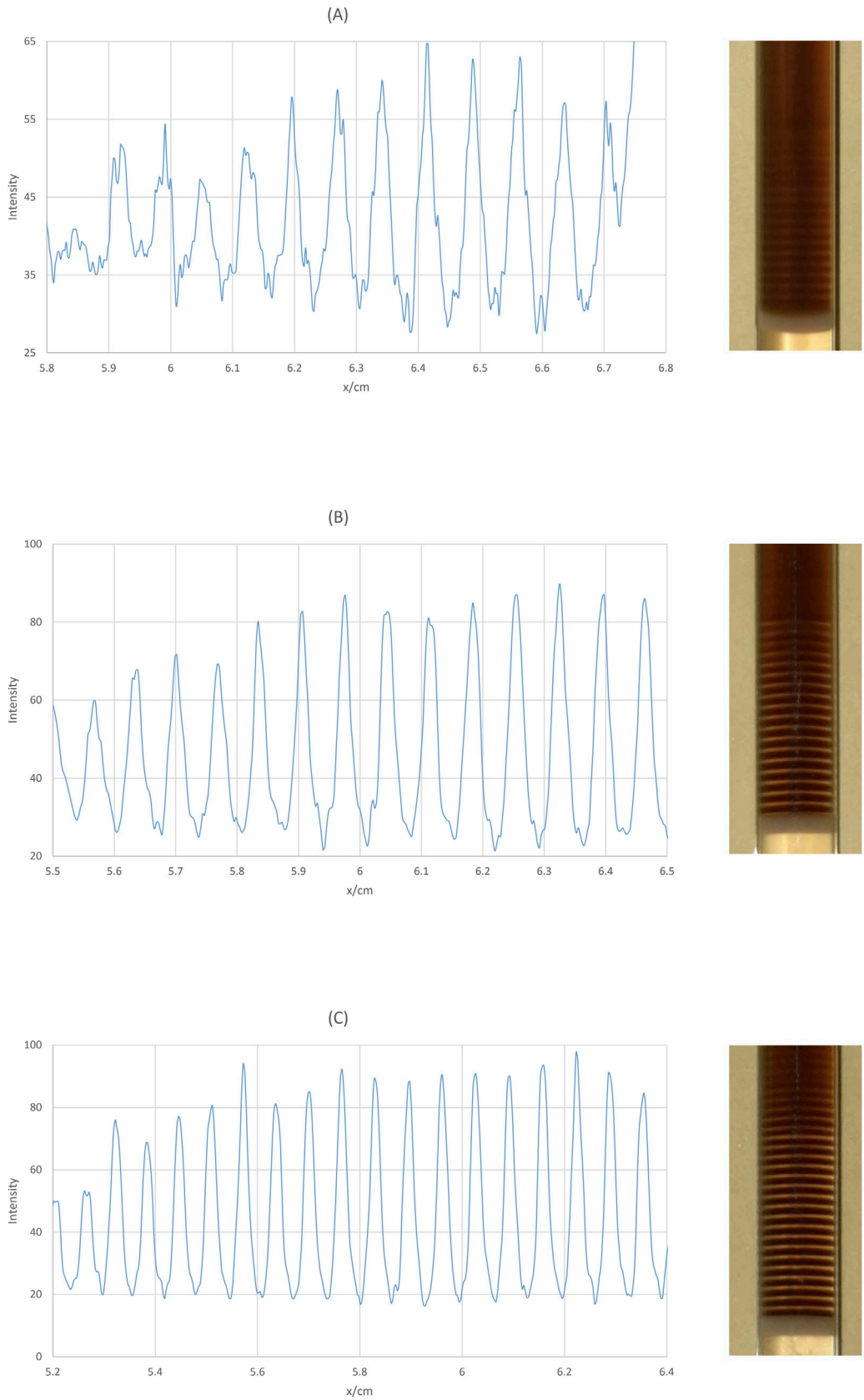


FIGURE 5
Intensity profiles for 2.5% gelatin, 1 M $Na_2S_2O_3{\cdot}5H_2O$ on Day 3 with **(A)** no KF added, **(B)** 0.01 M kF, and **(C)** 0.1 M kF.

TABLE 1 The values of the power law exponent $\alpha$ for the dependence of the migration extent $d$ on time, $d(t) \propto t^{\alpha}$.

| | | 0.01 M KF | | | | | | 0.1 M KF | | | | | |
|---|---|---|---|---|---|---|---|---|---|---|---|---|---|
| Gelatin | | 2.5% | 5% | 7.5% | 10% | 12.5% | 2.5% | 7.5% | 12.5% | 2.5% | 7.5% | 12.5% | |
| $Na_2S_2O_3{\cdot}5H_2O$ | | | | | | | | | | | | | |
| 0.1 M | | 0.440±0.006 | 0.512±0.006 | 0.539±0.006 | 0.539±0.007 | 0.547±0.007 | 0.482±0.006 | 0.532±0.006 | 0.537±0.006 | 0.484±0.006 | 0.531±0.006 | 0.557±0.006 | |
| 1 M | | 0.435±0.004 | 0.509±0.004 | 0.524±0.004 | 0.510±0.005 | 0.504±0.005 | 0.489±0.004 | 0.527±0.004 | 0.517±0.004 | 0.483±0.004 | 0.537±0.004 | 0.523±0.004 | |
| 2.5 M | | 0.426±0.004 | 0.500±0.004 | 0.514±0.004 | 0.522±0.004 | 0.421±0.003 | 0.481±0.004 | 0.524±0.004 | 0.549±0.004 | 0.476±0.004 | 0.535±0.004 | - | |

diffusion and affects the migration extent while the nucleation rate and band width are experimentally controlled by the gelatin concentration.

## 4.2 Silver sulfide $Ag_2S$

As diffusion of sodium thiosulfate continues along the reaction tube, the solution meets the silver thiosulfate band rear. When the thiosulfate ion concentration is sufficient to dissolve the $Ag_2S_2O_3$ precipitate, dissolution takes place and the soluble complex ion bis(thiosulfato) argentite $[Ag(S_2O_3)_2]^{3-}$ is formed. This dissolution depletes the region from $S_2O_3{}^{2-}$ ions. Until the following build-up of the thiosulfate ion concentration, the undissolved $Ag_2S_2O_3$ dissociates to $Ag_2S$. This repeated mechanism creates particularly for the 2.5% gelatin systems alternation of $[Ag(S_2O_3)_2]^{3-}$ soluble regions and $Ag_2S$ precipitate regions as diffusion progresses down the reaction tube. The features of the obtained pattern for a specific system are found to be fixed in location as presented in Figure 4 as an example. This behavior contrasts with the prenucleation model in which the positions of the bands are fixed at the nucleation and growth step. In the silver thiosulfate/silver sulfide system, the $Ag_2S$ bands are formed at $S_2O_3{}^{2-}$ depleted regions and the dissolution and thus the inter-band spacing is formed at regions where the outer electrolyte concentration is abundant. Upon increasing the gelatin percentage, the $Ag_2S$ pattern morphology changes from high density banding, to low density with no clear boundaries between the dissolved and precipitate regions as seen in Figure 1.

The impact of solvent polarity on the formation and morphology of the patters is studied by adding an inert salt potassium fluoride KF, to the inner electrolyte immobile solution. Even though in fully neutralized gels, the ionic term is not expected to play an explicit role on the structure and properties of the gel [39], nevertheless, the solvent polarity affects the stability of complex ions, and the stability of colloidal particles [40–43]. Thus, electrolyte-polymer gel interactions do not play a central role in the pattern formation; instead the effect of KF on the $[Ag(S_2O_3)_2]^{3-}$ complex ion and $Ag_2S$ colloidal particles affects the pattern formation. High ionic strength stabilizes complex ions by reducing repulsion between like-charged ligands, enhancing ligand exchange kinetics, and therefore making complexation more favorable. And with increasing solvent polarity, the attractive dispersion interactions decrease resulting in partial gain of colloid stability. These effects are demonstrated in the sharper boundaries between the precipitate and dissolved regions in systems with KF, compared to the KF free systems as seen for the 2.5% gelatin percentage high frequency Liesegang patterns and the better resolved doublets for the 7.5% gelatin systems and singlets for the 12.5% gelatin systems in the presence of KF, Figure 1.

Finally, the silver sulfide band width $w_n$ and the $[Ag(S_2O_3)_2]^{3-}$ inter band spacing $\Delta x_n$ for the most morphologically resolved 2.5% gelatin Liesegang patterns on Day 3 are determined by analyzing the spatial variations of the pixel intensity, as seen for the 1M $Na_2S_2O_3{\cdot}5H_2O$ systems in Figure 5 as examples. The intensity profiles gave uniform $Ag_2S$ band width independent of its location. In addition, the $[Ag(S_2O_3)_2]^{3-}$ inter band spacing was found to be equidistant, and independent of the inter band location. Values for the average band width and the average inter band spacing with the corresponding standard deviations are given in Table 2.

TABLE 2 Average $Ag_2S$ band width $w_n$ and average $[Ag(S_2O_3)_2]^{3-}$ inter band spacing $\Delta x_n$ for 2.5% gelatin systems.

| | | | | 0.01 M KF | | | 0.1 M KF | | |
|---|---|---|---|---|---|---|---|---|---|
| $Na_2S_2O_3{\cdot}5H_2O$ | 0.1 M | 1 M | 2.5 M | 0.1 M | 1 M | 2.5 M | 0.1 M | 1 M | 2.5 M |
| *avg.* $w_n$ [cm] | 0.025 | 0.045 | 0.051 | 0.025 | 0.050 | 0.047 | 0.023 | 0.043 | 0.046 |
| SD | 0.002 | 0.004 | 0.001 | 0.003 | 0.002 | 0.003 | 0.002 | 0.002 | 0.001 |
| *avg.* $\Delta x_n$ [cm] | 0.014 | 0.024 | 0.026 | 0.015 | 0.018 | 0.025 | 0.020 | 0.022 | 0.021 |
| SD | 0.003 | 0.003 | 0.004 | 0.003 | 0.002 | 0.002 | 0.001 | 0.001 | 0.002 |

Such uniformity diverges from classical Liesegang phenomena, which often exhibit progressively wider spacing. The constant inter band spacing suggests a silver thiosulfate dissolution mechanism that does not fluctuate significantly at the $Ag_2S_2O_3$ band tail due to diffusivity gradients like in typical Liesegang systems. The emergence of the equidistant pattern can be compared to the theoretical model by Lagzi and Kármán[7], where the formation of the bands is provoked by the propagation of the outer electrolyte which moves at a constant velocity. The dynamics of propagation maintains a constant concentration of the outer electrolyte and the formation of the precipitate band takes place when its local concentration reaches some threshold value. Another emphasis on the threshold concentration in obtaining equidistant patterns is found in the sol coagulation model [8]. Comparably, when the concentration of $Ag_2S$ precipitate, formed by the dissociation of $Ag_2S_2O_3$ due to the presence of water, reaches its threshold value, a band is formed. Meanwhile, and until the threshold of precipitation is reached again and another $Ag_2S$ precipitate band is formed, the silver thiosulfate dissolves in the excess available $Na_2S_2O_3$ solution forming the $Na_3[Ag(S_2O_3)_2]$*(aq)* inter-band region. The equidistant microscale $Ag_2S$ Liesegang pattern reflects an intrinsic regulatory mechanism rooted in the dissolution and dissociation dynamics in the gelatin medium. This consistent band width and spacing hint at potential applications in microscale templating or micro-patterning [44], where spontaneous bottom-up highly periodic structures are desirable.

The findings highlight the role of diffusion, ionic strength of the medium, and threshold concentration in the development of $Ag_2S$ patterns. The formation and colloid growth of silver sulfide are governed by physicochemical mechanisms [45, 46]. The findings can help reconstruct sulfide bearing fluids evolution pathways, infiltrating fractures or pores in silver bearing rocks responsible for silver sulfide deposition. Thus predicting locations of significant acanthite concentrations in geochemical systems.

## 5 Conclusion

In conclusion, the experimental investigation of silver thiosulfate $Ag_2S_2O_3$ formation within a gelatin matrix revealed a dynamic diffusion-controlled reaction confirmed by a square root time dependence. The migration extent of the $Ag_2S_2O_3$ band front decreases with increasing gelatin percentage due to reduced pore size and mobility in the gelatin, and increases with higher $Na_2S_2O_3$ concentrations due to stronger concentration gradients. The band width of the $Ag_2S_2O_3$ precipitate increases over time and with gelatin concentration due to increased surface area and density of the matrix creating more nucleation sites. At the rear of the $Ag_2S_2O_3$ band, dissolution into $[Ag(S_2O_3)_2]^{3-}$ complex ion or dissociation into $Ag_2S$ precipitate occurs depending on the thiosulfate ion availability. The alternating process particularly for the 2.5% gelatin systems led to spatially distinct zones, giving rise to equidistant silver sulfide Liesegang pattern. The morphology of the $Ag_2S$ bands, ranging from high-density bands to diffuse regions is predominantly dictated by the gelatin matrix. The impact of solvent polarity on the patterns appears in pattern sharpness, due to its influence on the complex ion and colloid stability. This system wherein the kinetics of dissolution and dissociation are alternating in response to the diffusion of a counter ion that initially forms a precipitate in the gelatin medium at the reaction front showcases a unique class of Liesegang patterns.

## Data availability statement

The original findings presented in the study are included in the article, further inquiries can be directed to the corresponding author.

## Author contributions

LB: Conceptualization, Data curations, Formal analysis, Investigation, Methodology, Validation, Writing – original draft, Writing – review and editing.

## Funding

The author(s) declared that financial support was received for this work and/or its publication. A funding support for the article processing charges was received from Notre Dame University - Louaize.

## Acknowledgements

The author thanks the Department of Sciences at Notre Dame University–Louaize for acquiring the chemicals and materials.

## Conflict of interest

The author(s) declared that this work was conducted in the absence of any commercial or financial relationships that could be construed as a potential conflict of interest.

## Generative AI statement

The author(s) declared that generative AI was not used in the creation of this manuscript.

Any alternative text (alt text) provided alongside figures in this article has been generated by Frontiers with the support of artificial intelligence and reasonable efforts have been made to ensure accuracy, including review by the authors wherever possible. If you identify any issues, please contact us.

## Publisher's note

All claims expressed in this article are solely those of the authors and do not necessarily represent those of their affiliated organizations, or those of the publisher, the editors and the reviewers. Any product that may be evaluated in this article, or claim that may be made by its manufacturer, is not guaranteed or endorsed by the publisher.

## References


1. Nabika H. Structural selection rules in self-assembly and self-organization: role of entropy production rate. *Bull Chem Soc Jpn* (2025) 98(6):uoaf048. doi:10.1093/bulcsj/uoaf048

2. Duzs B, Lagzi I, Szalai I. Reactor design for chemical reaction-diffusion systems. *ChemSystemsChem* (2025) 7(e00024):1–14. doi:10.1002/syst.202500024

3. Shvartsev SL. Self-organizing abiogenic dissipative structures in the geologic history of the Earth. *Earth Sci Front* (2009) 16(6). doi:10.1016/S1872-5791(08)60114-1

4. Ni H, Pan M, Shi K, Zhou J, Wu M. Preparation of isometric liesegang patterns and application in multi-pulsed drug release system. *J Sol-gel Sci Technol* (2019) 91. doi:10.1007/s10971-019-04931-6

5. Sugiawati VA, Vacandio F, Galeyeva A, Kurbatov AP, Djenizian T. Enhanced electrochemical performance of electropolymerized self-organized $TiO_2$ nanotubes fabricated by anodization of Ti grid. *Front Phys* (2019) 7:179. doi:10.3389/fphy.2019.00179

6. Liesegang RE. Ueber einige Eigenschaften von Gallerten. *Naturw Wochenschr* (1896) 11:353–362. doi:10.1007/BF01830142

7. Lagzi I, Kármán D. Equidistant precipitate pattern formation behind a propagating chemical front. *Chem Phys Lett* (2003) 372(5-6). doi:10.1016/S0009-2614(03)00524-4

8. Molnár F, Izsák F, Lagzi I. Design of equidistant and revert type precipitation patterns in reaction diffusion systems. *Phys Chem Chem Phys* (2008) 10(17). doi:10.1039/b715775d

9. Morsali M, Khan MTA, Ashirov R, Hollo G, Baytekin HT, Lagzi I, et al. Mechanical control of periodic precipitation in stretchable gels to retrieve information on elastic deformation and for the complex patterning of matter. *Adv Mater* (2020) 32(10):1905779. doi:10.1002/adma.201905779

10. Ezzeddine D, El-Rassy H, Sultan R. Surface and structural studies in a $PbCrO_4$ liesegang pattern with revert spacing. *Chem Phys Lett* (2019) 734:136735. doi:10.1016/j.cplett.2019.136735

11. Droz M, Magnin J, Zrinyi M. Liesegang patterns: studies on the width law. *J Chem Phys* (1999) 110. doi:10.1063/1.478927

12. Mora S, Pomeau Y. Brownian diffusion in a dilute field of traps in Fickean but Non-Gaussian. *Phys Rev E* (2018) 98(4):040101. doi:10.1103/PhysRevE.98.040101

13. Itatani M, Fang Q, Unoura K, Nabika H. Programmable design of self-organized patterns through a precipitation reaction. *J Phys Chem B* (2020) 124(38). doi:10.1021/acs.jpcb.0c05603

14. Ibrahim H, El-Rassy H, Sultan R. Liesegang bands *versus* random crystallites in $Ag_2Cr_2O_7$ - single and mixed gelled media. *Chem Phys Lett* (2018) 693:198–201. doi:10.1016/j.cplett.2018.01.014

15. Sultan R, Halabieh R. Effect of an electric field on propagating $Co(OH)_2$ Liesegang patterns. *Chem Phys Lett* (2000) 332(3-4):331–338. doi:10.1016/S0009-2614(00)01200-8

16. Badr L, Moussa Z, Hariri A, Sultan R. Band, target, and onion patterns in $Co(OH)_2$. Liesegang systems. *Phys Rev E* (2011) 83:016109. doi:10.1103/PhysRevE.83.016109

17. Holló G, Zámbó D, Deák A, Rossi F, Cucciniello R, Nostro PL, et al. Effect of the polarity of solvents on periodic precipitation: formation of hierarchical revert Liesegang patterns. *J Phys Chem B* (2022) 126(41). doi:10.1021/acs.jpcb.2c05810

18. Sultan RF, Abdel-Rahman AFM, Abdel-Rahman M. On dynamic self-organization: examples from magmatic and other geochemical systems. *Lat Am J Sol Struct.* (2013) 10(1):59–73. doi:10.1590/S1679-78252013000100006

19. Nakouzi E, Steinbock O. Self-organization in precipitation Reactions far from the Equilibrium. *Sci Adv* (2016) 2(8):e1601144. doi:10.1126/sciadv.1601144

20. Arı H, Uzunlar R, Akbulut ES, Lagzi I, Baytekin B. Chemical reactions with Liesegang rings: generation of non-permanent thermal patterns. *Soft Matter* (2025) 21(16). doi:10.1039/d4sm01074d

21. Jiang J, Sakurai K. Formation of Ultrathin liesegang patterns. *Langmuir* (2016) 32(36). doi:10.1021/acs.langmuir.6b02148

22. Nabika H, Itatani M, Lagzi I. Pattern formation in precipitation reactions: the Liesegang phenomenon. *Langmuir* (2020) 36(2):481–497. doi:10.1021/acs.langmuir.9b03018

23. Polezhaev AA, Müller SC. Complexity of precipitation patterns: Comparison of simulation with experiment. *Chaos* (1994) 4(4):631–636. doi:10.1063/1.166040

24. Veen H. Silver thiosulphate: an experimental tool in plant science. *Sci Hortic* (1983) 20(3):211–224. doi:10.1016/0304-4238(83)90001-8

25. Vladimirova L, Nedeltcheva T. Study of the potential of silver/sulfide ion selective electrode in solutions of silver and thiosulfate ions when the thiosulfate is in excess. *J Chem Technol Metall* (2016) 51(5):536–569.

26. Hyde PT, Guan X, Abreu V, Setter TL. The anti-ethylene growth regulator silver thiosulfate (STS) increases flower production and longevity in cassava (*Manihot esculenta* Crantz). *Plant Growth Regul* (2020) 90:441–453. doi:10.1007/s10725-019-00542-x

27. Ota A, Tajima M, Mori K, Sugiyama E, Sato VH, Sato H. The selective cytotoxicity of silver thiosulfate, a silver complex, on MCF-7 breast cancer cells through ROS-induced cell death. *Pharmacol Rep* (2021) 73(3):847–857. doi:10.1007/s43440-021-00260-0

28. Kissin SA, Mango H. Silver vein deposits. In: HD Holland, KK Turekian, editors. *Treatise on geochemistry*. Elsevier Science (2014). p. 425–432. doi:10.1016/B978-0-08-095975-7.01118-9

29. Syed S. Silver recovery aqueous techniques from diverse sources: hydrometallurgy in recycling. *Waste Management* (2016) 50:234–256. doi:10.1016/j.wasman.2016.02.006

30. Liang J, Wang T, Qiu P, Yang S, Ming C, Chen H, et al. Flexible thermoelectrics: from silver chalcogenides to full-inorganic devices. *Energy Environ. Sci.* (2019) 12. doi:10.1039/C9EE01777A

31. Subramani A, Vairapperumal T. Wearable thermoelectric silver sulfides: from materials to applications. *Next Mater* (2025) 7:100627. doi:10.1016/j.nxmate.2025.100627

32. Kundu M, Terabe K, Hasegawa T, Aono M. Effect of sulfurization conditions and post-deposition annealing treatment on structural and electrical properties of silver sulfide films. *J Appl Phys* (2006) 99(10):103501. doi:10.1063/1.2199067

33. Hada H, Yonezawa Y, Yoshida A, Kurakake A. Photoreduction of silver ion in aqueous and alcoholic solutions. *J Phys Chem* (1976) 80(25). doi:10.1021/j100566a003

34. Schindelin J, Arganda-Carreras I, Frise E, Kaynig V, Longair M, Pietzsch T, et al. Fiji: an open-source platform for biological-image analysis. *Nat Methods* (2012) 9(7):676–682. doi:10.1038/nmeth.2019

35. Starink MJ. A new model for diffusion-controlled precipitation reactions using the extended volume concept. *Thermochim Acta* (2014) 596:109–119. doi:10.1016/j.tca.2014.09.016

36. Maaloum M, Pernodet N, Tinland B. Agarose gel structure using atomic force microscopy: gel concentration and ionic strength effects. *Electrophoresis* (1998) 19(10). doi:10.1002/elps.1150191015

37. Nindiyasari F, Fern´andez-Díaz L, Griesshaber E, Astilleros JM, Sanchez- Pastor N, Schmahl WW. Influence of gelatin Hydrogel porosity on the crystallization of $CaCO_3$. *Cryst Growth Des* (2014) 14(4). doi:10.1021/cg401056t

38. Badr L, Epstein IR. Size-controlled synthesis of $Cu_2O$ nanoparticles via reaction-diffusion. *Chem Phys Lett* (2017) 669:17–21. doi:10.1016/j.cplett.2016.11.050

39. Zhang L, Mikhailovskaya A, Constantin D, Foffi G, Tavacoli J, Schmitt J, et al. Varying the counter ion changes the kinetics, but not the final structure of colloidal gels. *J Colloid Interf Sci.* (2016) 463:137–144. doi:10.1016/j.jcis.2015.10.046

40. Dash UN. Solute–solvent interactions and dissolution of some sparingly soluble silver salts in various solvent systems. *Fluid Phase Equilib* (1981) 5(3-4):323–326. doi:10.1016/0378-3812(80)80064-1

41. Dembek M, Bocian S, Buszewski B. Solvent influence on zeta potential of stationary phase-mobile phase interface. *Molecules* (2022) 27(3):968. doi:10.3390/molecules27030968

42. Israelachvili JN. *Intermolecular and surface forces*. Cambridge, Massachusetts, United States: Academic Press (2011). p. 227. doi:10.1016/C2009-0-21560-1

43. Matsue M, Itatani M, Fang Q, Shimizu Y, Unoura K, Nabika H. Role of electrolyte in Liesegang pattern formation. *Langmuir* (2018) 34(37):11188–11194. doi:10.1021/acs.langmuir.8b02335

44. Itatani M, Onishi Y, Suematsu NJ, Lagzi I. Periodic precipitation in a confined liquid layer. *J Phys Chem Lett* (2024) 15(18):4948–4957. doi:10.1021/acs.jpclett.4c00832

45. Fontbote L, Kouzmanov K, Chiaradia M, Pokrovski GS. Sulfide minerals in hydrothermal deposits. *Elements* (2017) 13:97–103. doi:10.2113/gselements.13.2.97

46. Fu X, Niu Z, Peng C, Han H, Sun W, Yue T. Quantitative synergistic adsorption affinity of Ca(II) and sodium oleate to predict the surface reactivity of hematite and quartz. *Sep Purif Techno* (2025) 360:131196. doi:10.1016/j.seppur.2024.131196